Metal–Organic Frameworks

DOI: 10.1002/anie.201410459

The Structure of the Aluminum Fumarate Metal–Organic Framework A520**

Elsa Alvarez, Nathalie Guillou, Charlotte Martineau, Bart Bueken, Ben Van de Voorde, Clément Le Guillouzer, Paul Fabry, Farid Nouar, Francis Taulelle, Dirk de Vos, Jong-San Chang, Kyoung Ho Cho, Naseem Ramsahye, Thomas Devic, Marco Daturi, Guillaume Maurin, and Christian Serre**

Abstract: *The synthesis of the commercially available aluminum fumarate sample A520 has been optimized and its structure analyzed through a combination of powder diffraction, solid-state NMR spectroscopy, molecular simulation, IR spectroscopy, and thermal analysis. A520 is an analogue of the MIL-53(Al)-BDC solid, but with a more rigid behavior. The differences between the commercial and the optimized samples in terms of defects have been investigated by in situ IR spectroscopy and correlated to their catalytic activity for ethanol dehydration.*

Metal–organic frameworks[1] (MOFs) have been extensively studied during the past two decades, and thousands of different architectures built up from almost all elements of the periodic table, and a large diversity of organic linkers now exist. To date, these micro- or mesoporous solids have been evaluated for a wide range of applications,[2] including gas storage, separation, heat transfer, catalysis, sensing, biomedicine and many others. Six MOFs are currently commercialized by BASF and Sigma–Aldrich; all of them are porous metal carboxylates or imidazolates.[3–5] However, to the best of our knowledge, only two MOFs have been promoted to the level of commercial applications. A dense zinc glutarate[6] is currently used as an epoxide-polymerization catalyst, while the microporous aluminum fumarate A520[7] is employed as a sorbent to store and deliver natural gas for automotive applications.[5]

This latter solid shows several advantages: 1) low cost associated with the use of a potentially renewable dicarboxylic linker and an abundant metallic cation; 2) good water stability; 3) an environmentally friendly synthesis route, which involves only water and simple aluminum salts; and 4) a large scale production, with a record space–time yield of 3,600 $kg\,m^{-3}\,day^{-1}$. Although A520 is one of the most promising MOFs in terms of applications, its poor crystallinity is still a severe obstacle to obtain the structure solution for this solid. Indeed, the structure elucidation of a polycrystalline solid is a prerequisite not only for an understanding of its properties, but also for guiding further optimization of its synthetic conditions. This requires X-ray diffraction data of sufficient quality and thus calls for the highest possible crystallinity of the sample, especially for indexing the corresponding powder diffraction pattern, which is a critical step for an accurate structural determination. Such an objective would not have been possible without amending the existing synthesis route of A520.

To achieve a better control over the nucleation, a gentle method to gradually increase the pH of the reaction mixture was developed by replacing the direct mixing of fumaric acid and NaOH with a slow decomposition of urea in hot water. This enables better control of crystallites growth, leading to a polycrystalline solid with a much better crystallinity compared to the initial recipe (Supporting Information, Figures S3–S5). Nevertheless, despite the larger particle size

[*] E. Alvarez, N. Guillou, C. Martineau, P. Fabry, F. Nouar, F. Taulelle, T. Devic, C. Serre
Institut Lavoisier de Versailles, UMR 8180 CNRS
Université de Versailles
45 Avenue des Etats Unis, 78035 Versailles cedex (France)
E-mail: christian.serre@uvsq.fr

E. Alvarez, C. Le Guillouzer, M. Daturi
Laboratoire Catalyse et Spectrochimie, ENSICAEN
Université de Caen, CNRS
6, Bd Maréchal Juin, 14050 Caen (France)

E. Alvarez
PSA Peugeot Citroën—Direction Scientifique et Technologies Futures. DSTF/SEPC/STEP
Route de Gisy, 78943 Velizy-Villacoublay cedex (France)

N. Ramsahye, G. Maurin
Institut Charles Gerhardt Montpellier UMR 5253 CNRS
UM ENSCM, Université Montpellier
Place E. Bataillon, 34095 Montpellier cedex 05 (France)
E-mail: gmaurin@univ-montp2.fr

B. Bueken, B. Van de Voorde, D. de Vos
Centre for Surface Chemistry and Catalysis
Katholieke Universiteit Leuven
Kasteelpark Arenberg 23, 3001 Leuven (Belgium)

J.-S. Chang, K. H. Cho
Catalysis Center for Molecular Engineering
Korea Research Institute of Chemical Technology (KRICT)
Jang-dong 100, Yuseong, Daejeon 305-600 (South Korea)

J.-S. Chang
Department of Chemistry, Sungkyunkwan University
Suwon 440-476 (South Korea)

[**] J.-S.C. and K.H.C. are grateful to the Global Frontier Center for Hybrid Interface Materials (GFHIM) for its financial support (Grant No. NRF-2013M3A6B1078879). G.M. thanks Institut Universitaire de France for its support. M.D. is grateful to KRICT for financial support through the Institutional Collaboration Research Program (KK-1407A46).

Supporting information for this article is available on the WWW under http://dx.doi.org/10.1002/anie.201410459.

(ca. 1 μm instead of 0.1 μm), anisotropic peak broadening and peak overlaps were observed regardless of the synthesis parameters that were evaluated. This prevented any precise determination of peak positions and unambiguous pattern indexing.

Previous studies have however suggested that this aluminum fumarate would possess the same structure type as the one of MIL-53(Al) (1,4 BDC) MOF, but without any structural confirmation.[7] Based on our expertise with the flexible MIL-53-BDC solids,[8,9] we nevertheless selected a solution for the hydrated aluminum fumarate solid, among those proposed by pattern indexing. This led to a monoclinic cell with the $P2_1/c$ (no. 14) space group: a = 6.842(3) Å, b = 12.088(3) Å, c = 14.207(1) Å, β = 122.55(1)°, V = 990(1) Å^3 (Supporting Information, Table S1). The same space group was obtained from previous reinvestigations of the MIL-53-BDC hydrated form.[10,11] At the first step of the structural determination, direct methods were used, leading to the location of Al atoms and most of the C and O atoms. A structural model was thus built up and subsequently optimized by density functional theory (DFT) calculations (see the Supporting Information). These simulations were performed by considering the presence of water in the pores (ca. 3.5 H_2O/Al, as determined by TGA) and by allowing a full relaxation of both the atomic positions and the cell parameters (Supporting Information, Tables S1, S2), Finally, the DFT-optimized framework structure was used as a starting point for further Rietveld refinement while the free water molecules were localized through successive difference Fourier maps. This led to a satisfactory structural model of this MIL-53(Al)-FA (FA for fumaric acid) as shown by the Rietveld plot (Supporting Information, Figure S1).

MIL-53(Al)-FA, with the formula Al(OH)(fum)·x H_2O (x = 3.5; fum = fumarate) exhibits a structure that is indeed isoreticular to that of the well-known material MIL-53(Al)-BDC or Al(OH)(BDC)·H_2O (BDC = 1,4-benzenedicarboxylate). The framework is built up from chains of corner-sharing metal octahedra linked together by fumarate to form lozenge-shaped 1D pores having circa 5.7 × 6.0 Å^2 free dimensions (Figure 1). As expected, these sizes are smaller than those observed for the parent terephthalate open forms (7.3 × 7.7 Å^2 for MIL-53(Al)-BDC *as* (*as* for as-synthesized) and 8.5 × 8.5 Å^2 MIL-53(Al)-BDC *ht*) (*ht* for high temperature), consistent with the shorter length of the fumaric acid compared to terephthalic acid[9] (see pore size distributions in the Supporting Information). The DFT predicted structure (Supporting Information, Figure S26) reveals that the water molecules are arranged in such a way to form hydrogen bonds with the framework between 1) their oxygen atoms O_w and the proton of the μ_2-OH functions and 2) their protons H_w and the oxygen atoms of the carboxylate group O_c. The characteristic distances between two water/host oxygen atoms range from 2.82 and 3.04 Å, which fit well with those evidenced from the experimentally-refined structure (Supporting Information, Figure S26). The confined water molecules form a relatively strong hydrogen bond network with corresponding O_w–O_w distances (from 2.71 to 2.91 Å) as short as those usually observed for water in bulk state. This spatial distribution and the interactions in play are reminiscent of

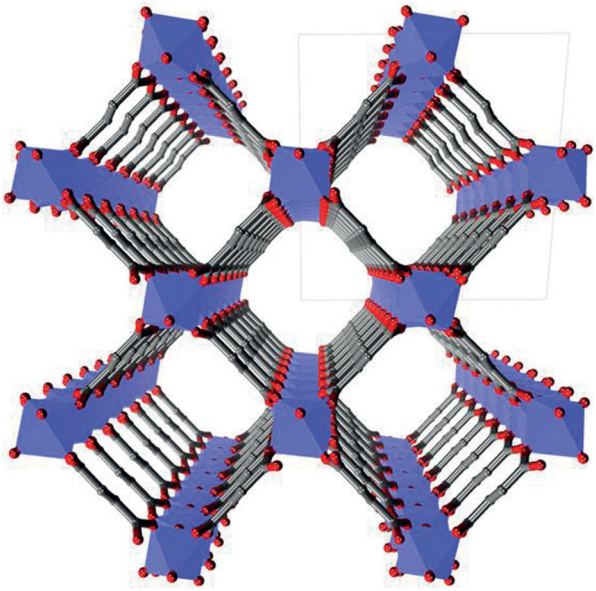

Figure 1. a) View along the *a* axis of the A520 structure. Al octahedra blue, O red, C gray. Hydrogen atoms have been omitted for clarity.

those previously observed in the MIL-53 series.[12] To obtain an insight into the structure at the microscopic level, solid-state NMR and IR spectroscopy experiments were carried out on both BASF Basolite A520 and MIL-53(Al)-FA; these data were compared to those previously obtained for the hydrated form of MIL-53(Al)-BDC. The shape of the ^{27}Al (a quadrupolar nucleus) MAS NMR spectra (Figure 2) of the hydrated A520 solids (quadrupolar coupling constant C_Q of 11.2 MHz, asymmetry parameter η_Q of 0.10) is similar to that observed for hydrated MIL-53(Al)-BDC (C_Q = 10.7 MHz, η_Q = 0.15). This observation is consistent with Al atoms

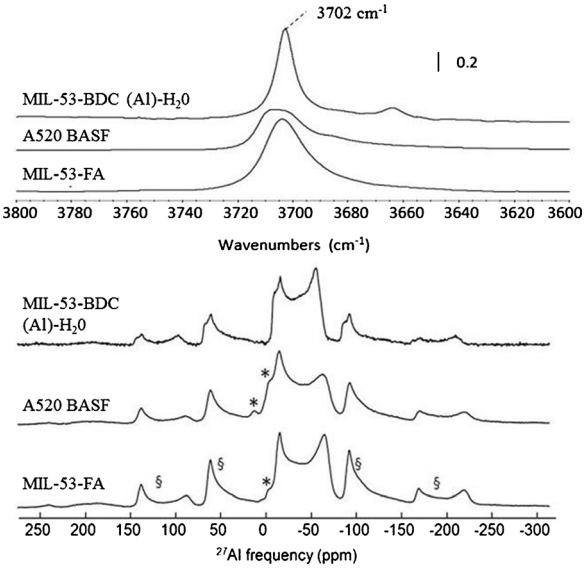

Figure 2. Top: Absorbance IR spectra of the hydrated Al fumarate solids and MIL-53-BDC(Al)-H_2O. Bottom: ^{27}Al solid-state MAS NMR spectra of MIL-53-BDC (Al)-H_2O and the Al fumarate solids (hydrated forms). ⋆ denotes the Al oxide/hydroxide impurities, as confirmed by the ^{27}Al MQMAS spectrum of MIL-53(Al)-FA shown in the Supporting Information, Figure S9. § symbols denote spinning sidebands.

coordinated octahedrally and with the octahedra sharing opposite corners.[9] The first-principles calculations of the NMR parameters using the DFT-optimized structural model for $x = 3.5\,H_2O$ led to two nonequivalent Al sites: a first one, with $C_Q = 11.5$ MHz, in very good agreement with the experimental findings, and a second population, with a lower C_Q of 7.9 MHz, which is very close to the NMR parameter previously reported for the dehydrated MIL-53(Al)-BDC ($C_Q = 8.3$ MHz; Supporting Information, Figure S8). In the A520 case, this second ^{27}Al site can be explained by the partially hydrated state considered in our structural DFT model. To illustrate this, further experiments were recorded on the solids after overnight dehydration at 100 °C. The resulting ^{27}Al C_Q value is lower (8.7 MHz) than in the initial hydrated phase, as previously observed for MIL-53(Al)-BDC, while the η_Q value remains close to 0.10. This C_Q value is very close to that obtained by DFT for the second population of Al in the partially hydrated DFT structure model, corroborating our findings. Moreover the dehydration–rehydration of the Al fumarate is reversible, as shown by the solid-state NMR data presented in the Supporting Information, Figure S7.

The bridging OH groups are observed in the ^{1}H MAS NMR spectra at 1.75 ppm (Supporting Information, Figure S6), as well as in the IR spectra with the signature of the $\nu(\mu_2\text{-OH})$ band at about 3650–3700 cm^{-1}, which is typical for the corner-sharing chains of metal octahedra.[11] Note that a small fraction of inorganic Al oxy-hydroxide impurity is present in both solids, however to a much smaller extent in the optimized sample. This was also confirmed by TGA (Supporting Information, Figure S13).

As the MIL-53-BDC solid is known to be highly flexible, the thermal behavior of the title solid was investigated by temperature-dependent X-ray powder diffraction and thermogravimetric analysis (Supporting Information, Figure S13). Unlike the parent terephthalate form, the Al fumarate exhibits on the whole a rigid character during the dehydration process. No drastic shift of the Bragg peaks occurs upon the loss of free water molecules. Indeed, the 0*kk* reflections are mostly affected with a small shift to higher angles. This suggests a very small contraction (lower than 1%) of the channel along the fumarate direction. Moreover, this is combined with a large broadening effect of the Bragg peaks, which makes refinement of the unit cell parameters for the anhydrous compound impossible. Indeed, the full width at half maximum (FWHM) of the (011) reflection of the hydrated form increases from 0.084 to 0.226°(2θ). This crystallinity loss is reversible upon rehydration, showing that broadening effect should be attributed to large strains in the dehydrated material (Figure 3). This might be due to the more rigid character of the fumarate linker compared to the terephthalate one, as the flexibility of MIL-53(Al)-BDC is typically associated with the rotation, as a knee-cap, of the linker around the axis of the chains. This rotation, possible with the aromatic ring, cannot take place for the fumarate conjugated system.[13]

The porosity of the Al fumarate in its dehydrated state was determined by nitrogen porosimetry at 77 K. The experimental BET area of 1080 m^{2}g^{-1} for MIL-53(Al)-FA,

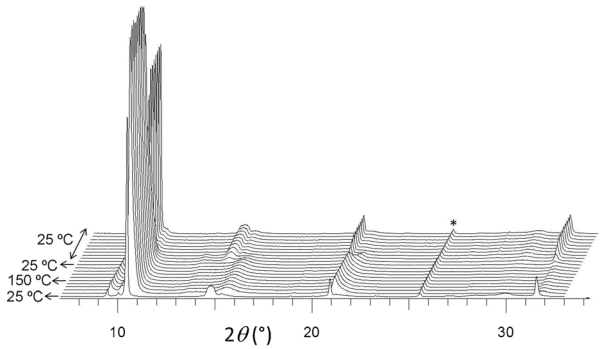

Figure 3. X-ray temperature-dependent powder diffraction of MIL-53(Al)-FA (air atmosphere; Cu radiation) from 25 to 150 °C followed by rehydration at 25 °C for 5 h. Note the presence of the Kβ contribution of the main peak at 2θ close to 9°. ⋆ denotes the sample holder.

is slightly higher than for BASF Basolite A520 by about 70 m^{2}g^{-1} (Supporting Information, Figures S10–S12). This observation emphasizes the absence of a significant amount of inorganic impurities for MIL-53(Al)-FA. TGA indicates also weight losses, in excellent agreement with the formula deduced from the structure determination (see the Supporting Information).

Ethanol is one of the future biobased feedstocks, obtained by fermentation, and can be transformed to ethylene or other intermediates, for instance on molecular sieves or on alumina based catalysts.[14] Interestingly, the conversion of ethanol is also a sensitive probe reaction to characterize catalytic surface sites, with the product distribution being determined by the nature of the sites and the temperature.[15–17] Table 1 reports product selectivities at near-equal ethanol conversions using various Al fumarates. As expected, the structure of A520 type materials is quite resistant to the temperatures (250-300 °C) at which the reaction was conducted.

Table 1: Conversion (*X*) of ethanol and product selectivity (*S*) of the Al fumarates A520 and MIL-53(Al)-FA at 300 °C.[a]

Sample	X [%]	S_{ET}[b] [%]	S_{DEE}[c] [%]	S_{ACD}[d] [%]	S_{others} [%]
BASF A520	9.2	12.3	43.0	40.1	4.6
MIL-53(Al)-FA	10.7	11.9	61.9	21.0	5.2
γ-Al_2O_3[e]	23.9	9.2	89.3	0.9	0.6

[a] 100 mg catalyst activated overnight at 150 °C under N_2, 300 °C, 3 mL min^{-1} flow, 4.1 mmol/(g catalyst h) ethanol. [b] ET for ethylene. [c] DEE for diethylether. [d] ACD for acetaldehyde. Standard deviation on conversion ≤ 0.5%; Standard deviation on selectivity ≤ 1.2%. [e] catalyst amount adjusted to 32 mg, corresponding to the same amount of Al.

At an ethanol conversion of about 10%, diethyl ether and acetaldehyde are formed over A520 with comparable selectivities of about 40%, together with a minor amount of ethylene (9–11%). The formation of diethyl ether is related to the presence of weak Brønsted acid sites, as expected for a material with pores which are richly decorated with OH groups. Note that under similar conditions, diethyl ether is the dominant product (ca. 90% selectivity) when γ-alumina is used as the catalyst. Ethylene is especially formed at higher temperatures, on moderate to strong Brønsted acid sites. On

the other hand, dehydrogenation to acetaldehyde is known to occur in the presence of Lewis acid sites.[15,16,18] As no such sites are expected in a perfectly crystalline A520, the formation of acetaldehyde is a direct indication for the presence of structural defects. Remarkably, on the MIL-53(Al)-FA, the diethylether-acetaldehyde selectivity switches to about 60:20, instead of about 40:40 on the non-optimized material. This confirms that MIL-53(Al)-FA contains a much smaller concentration of defect sites with dehydrogenating capability. The same conclusion was obtained by in situ IR spectroscopy tests, which provide evidence that the optimized sample bears mostly Brønsted sites (Supporting Information, Figures S14–S20). Such defects could arise from missing linkers, leading to open Al sites (Supporting Information, Figure S21).

Finally, the microwave-assisted synthesis of the Al fumarate solids was investigated using both the BASF Basolite A520 and MIL-53(Al)-FA conditions. The BASF Basolite A520 condition was not effective under microwave irradiation because the use of a strong base, NaOH, induces the partial precipitation of the Al precursor into the corresponding hydroxide together with the formation of the Al fumarate phase. By contrast, the use of a mild base, urea, increased the crystallinity as well as the formation rate of the Al fumarate phase under microwave conditions by preventing the precipitation into the hydroxide (Supporting Information, Figure S22). Moreover, the microwave synthesis of MIL-53(Al)-FA led to a very high space–time yield (STY, 15200 $kg\,m^{-3}\,day^{-1}$) which is much higher than that (2450 $kg\,m^{-3}\,day^{-1}$) of A520 synthesized under hydrothermal conditions (Supporting Information, Table S5).[5] This high STY could later pave the way toward the exploration of a continuous microwave synthesis as an alternative production method of the Al fumarate.

In conclusion, using a slightly modified synthesis route compared with the initial conditions from BASF, a more crystalline aluminum fumarate sample was obtained which allowed us, based on a joint XRPD and computational approach, to propose for the first time a structural model reminiscent of the one of the MIL-53(Al)-BDC architecture. This hypothesis was further supported by data from solid-state NMR and IR spectroscopy experiments, coupled again with computations. It is noteworthy that, unlike its MIL-53(Al)-BDC analogue, it was found that the Al fumarate, denoted MIL-53(Al)-FA, exhibits a rigid character with an accessible permanent porosity. It was shown that the commercial sample possesses a higher degree of defects, leading to a different selectivity in ethanol dehydration.

Experimental Section

All chemicals and solvents were purchased from commercial sources and were used without further purification.

Routine X-ray powder diffraction (XRPD) patterns (Supporting Information, Figure S3) were collected at 293 K on a Siemens D5000 Diffractometer working in the (θ–2θ) by using Cu K_α radiation (λ = 1.5418 Å). XRPD used for structural determination was scanned at room temperature on a Bruker D8 Advance diffractometer equipped with a Ge(111) monochromator producing Cu $K_{\alpha1}$ radiation (λ = 1.540598 Å) and a LynxEye detector. The pattern was scanned at room temperature with a Debye–Scherrer geometry, in the 2θ range 5–90° (see more details on structural investigation in the Supporting Information). X-Ray thermodiffractometry was performed using a θ–θ Bruker-D8 Advance diffractometer equipped with a HTK-1200N (Anton Parr) temperature chamber and a LYNXEYE XE detector (Cu radiation). Diagrams were collected every 25 °C between 25 and 150 °C.

The solid-state magic-angle spinning (MAS) NMR spectra were recorded on an Avance Bruker 500 spectrometer (Larmor frequencies of 500.1 MHz for ^{1}H). The ^{1}H and ^{27}Al MAS (10 kHz) NMR spectra were recorded using a 90°-180°-90° Hahn-echo sequence, with inter-pulse delay synchronized with one rotor period. The 90° pulse lengths were set to 3 and 3.2 ms for ^{1}H and ^{27}Al, respectively. The ^{1}H–^{13}C cross-polarization (CPMAS) NMR spectra were recorded using a 5 ms contact time, and radio-frequency (rf) fields of 50 kHz on ^{13}C and 60 kHz on ^{1}H channel. ^{1}H SPINAL-64 decoupling (rf of 70 kHz) was used during acquisition of the ^{13}C CPMAS NMR spectra. The ^{1}H and ^{13}C chemical shifts were referenced to TMS, and the ^{27}Al chemical shifts were referenced to a 0.1 M solution of $Al(NO_3)_3$ at 0 ppm. The spectra were analyzed using the DMfit software.

The DFT calculations were performed with the Quickstep module, available as part of the CP2K code using the PBE functional and the triple zeta basis set (TZVP-MOLOPT) for all atoms, except for the Al centers, where double zeta functions (DZVP-MOLOPT) were employed. Semi-empirical dispersion corrections as implemented in the DFT-D3 method were considered.

Morphologic analysis of the crystals was carried out with a field-emission gun scanning electron microscope (FEG-SEM) JEOL JAMP 9500F (JEOL GmbH, Germany).

Thermogravimetric analyses were performed on a PerkinElmer, STA 6000 apparatus under O_2 flow between room temperature and 800 °C in an aluminum crucible (heating speed 3 °C min^{-1}) using 5–10 mg of products.

Specific surface area experiments were performed at 77 K on a Belsorp Mini apparatus using nitrogen as the probing gas, after a Belsorp Prep treatment overnight at 150 °C under primary vacuum (BEL Japan).

The samples (4–5 mg) for Fourier-transform infrared (FTIR) spectroscopy were deposited on a silicon wafer after dilution in ethanol. This was carried out to observe all structural bands clearly and sharply in the IR spectrum. The mixture was dried in air and placed in an IR quartz cell equipped with KBr windows. A movable quartz sample holder permits adjustment of the sample in the IR beam for acquisition of spectra and to displace it into a furnace at the top of the cell for thermal treatments. The cell is connected to a vacuum line for evacuation and calcination. IR spectra were recorded on a Thermo Scientific Nicolet 6700 spectrometer equipped with a DTGS detector. The resolution was 4 cm^{-1} and 64 scans were co-added for each spectrum, in a wavenumber range of 400–4000 cm^{-1}. In CO adsorption experiments, the temperature of the pellet was decreased to about 100 K by cooling the sample holder with liquid N_2 after quenching the sample from the thermal treatment temperature. The addition of accurately known increments of CO in the cell was possible by a calibrated volume (1.75 cm^3) connected to a pressure gauge for the control of the probe pressure (10^{-1}–10^4 Pa range). Prior to each adsorption measurement, the A520 solids were heated at 250 °C under secondary vacuum (10^{-3} Pa) during 5 h.

Received: October 25, 2014
Revised: December 17, 2014
Published online: February 4, 2015

Keywords: aluminum fumarate · metal–organic frameworks · modeling · solid state NMR spectroscopy · X-ray diffraction

[1] G. Férey, *Chem. Soc. Rev.* **2008**, *37*, 191 – 214.

[2] Themed issues: metal-organic frameworks, a) *Chem. Rev.* **2012**, *112*, 673 – 1268; b) *Chem. Soc. Rev.* **2014**.
[3] A. U. Czaja, N. Trukhan, U. Müller, *Chem. Soc. Rev.* **2009**, *38*, 1284 – 1293.
[4] U. Mueller, M. Schubert, F. Teich, H. Puetter, K. Schierle-Arndt, J. Pastré, *J. Mater. Chem.* **2006**, *16*, 626 – 636.
[5] M. Gaab, N. Trukhan, S. Maurer, R. Gummaraju, U. Müller, *Microporous Mesoporous Mater.* **2012**, *157*, 131 – 136.
[6] U. Mueller, G. Luinstra, O. M. Yaghi, US Pat. 6 617 467, **2004**, BASF Aktiengesellschaft.
[7] a) E. Leung, U. Müller, G. Cox, H. Mattenheimer, S. Blei, EP Patentanmeldung 10183283.0, **2010**; b) F. Jeremias, D. Fröhlich, C. Janiak, S. K. Henninger, *RSC Adv.* **2014**, *4*, 24073 – 24082.
[8] C. Serre, F. Millange, C. Thouvenot, M. Noguès, G. Marsolier, D. Louër, G. Férey, *J. Am. Chem. Soc.* **2002**, *124*, 13519 – 13526.
[9] T. Loiseau, C. Serre, C. Huguenard, G. Fink, F. Taulelle, M. Henry, T. Bataille, G. Férey, *Chem. Eur. J.* **2004**, *10*, 1373 – 1382.
[10] a) F. Millange, N. Guillou, R. I. Walton, J. M. Grenèche, I. Margiolaki, G. Férey, *Chem. Commun.* **2008**, 4732 – 4734; b) G. Ortiz, G. Chaplais, J.-L. Paillaud, H. Nouali, J. Patarin, J. Raya, C. Marichal, *J. Phys. Chem. C* **2014**, *118*, 22021 – 22029.
[11] C. Volkringer, T. Loiseau, N. Guillou, G. Férey, E. Elkaïm, A. Vimont, *Dalton Trans.* **2009**, 2241 – 2249.
[12] a) S. Bourrelly, B. Moulin, A. Rivera, G. Maurin, S. Devautour-Vinot, C. Serre, T. Devic, P. Horcajada, A. Vimont, G. Clet, M. Daturi, J.-C. Lavalley, S. Loera-Serna, R. Denoyel, P. L. Llewellyn, G. Férey, *J. Am. Chem. Soc.* **2010**, *132*, 9488 – 9498; b) N. Guillou, F. Millange, R. Walton, *Chem. Commun.* **2011**, *47*, 713 – 715.
[13] I. Alkorta, I. Rozas, J. Elguero, *J. Chem. Soc. Perkin Trans. 2* **1998**, 2671 – 2675.
[14] M. Zhang, Y. Yu, *Ind. Eng. Chem. Res.* **2013**, *52*, 9505 – 9514.
[15] H. Idriss, E. G. Seebauer, *J. Mol. Catal. A* **2000**, *152*, 201 – 212.
[16] C. L. Kibby, W. Keith Hall, *J. Catal.* **1973**, *29*, 144 – 159.
[17] A. Gervasini, J. Fenyvesi, A. Auroux, *Catal. Lett.* **1997**, *43*, 219 – 228.
[18] E. Iglesia, D. G. Barton, J. A. Biscardi, M. J. L. Gines, S. L. Soled, *Catal. Today* **1997**, *38*, 339 – 360.

